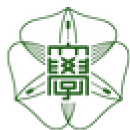
HOKKAIDO UNIVERSITY

Title	Fabrication and Characterization of GaAs Single Electron Devices Having Single and Multiple Dots Based on Schottky In-Plane-Gate and Wrap-Gate Control of Two-Dimensional Electron Gas
Author(s)	Kasai, Seiya; Jinushi, Kei-ichiroh; Tomozawa, Hidemasa; Hasegawa, Hideki
Citation	Japanese Journal of Applied Physics. Pt. 1, Regular papers, short notes & review papers, 36(3B), 1678-1685 https://doi.org/10.1143/JJAP.36.1678
Issue Date	1997-03
Doc URL	http://hdl.handle.net/2115/33085
Rights	Copyright © 1997 The Japan Society of Applied Physics
Type	article (author version)
File Information	kasai.pdf

Instructions for use

Hokkaido University Collection of Scholarly and Academic Papers : HUSCAP

Fabrication and Characterization of GaAs Single Electron Devices Having Single and Multiple Dots Based on Schottky In-Plane-Gate and Wrap-Gate Control of Two-Dimensional Electron Gas

Seiya KASAI, Kei-ichiroh JINUSHI, Hidemasa TOMOZAWA and
Hideki HASEGAWA
Research Center for Interface Quantum Electronics and Graduate School of Electronics and Information Engineering, Hokkaido University, Sapporo 060, Japan

(Received September 18, 1996; accepted for publication November 29, 1996)

Single-dot and multiple (2, 3, 18, and 37)-dot single electron transistors (SETs) based on the control of a two-dimensional electron gas (2DEG) with a recently proposed Schottky in-plane gate (IPG) and a newly introduced Schottky wrap gate (WPG) were successfully fabricated on AlGaAs/GaAs wafers using electron beam (EB) lithography and their transport properties were investigated. Each of the fabricated SETs showed Coulomb blockade-like conductance oscillation. In single-dot SETs, a strong correlation was found between the device dimensions and the temperature limit of conductance oscillation. Conductance oscillation characteristics of multiple-dot SETs were complicated, and were not explained by the classical Coulomb blockade theory. Based on a simplified theoretical analysis using computer simulation, it was shown that quantized energy due to electron confinement and dot-coupling can dominate the charging effect in the fabricated SETs.

KEYWORDS: single electron transistors, Schottky in-plane gate (IPG), Schottky wrap gate (WPG), single-quantum dot, multiple-quantum dot, Coulomb blockade

1. Introduction

With the recent rapid progress of fabrication techniques for nanostructures, various new phenomena related to single electron transport through single-[1] and multiple-quantum dots[2-8] have been identified and predicted. They are extremely interesting not only from the viewpoint of basic physics, but also from the engineering viewpoint of constructing next-generation electronics based on single-electron devices with new system architectures.

For the latter purpose, however, high-temperature operation of single-electron devices seems to be a requirement. Recently, great progress has been made towards room-temperature operation of Si-based single-electron transistors (SETs).[9,10] However, the GaAs-based SETs reported on so far operate mostly in the mK range, despite the fact that the first demonstration of the feasibility of semiconductor SETs was made using them.[11,12] This is primarily because of the split gate potential control used in GaAs-based SETs which produces a rather weak and gradual confinement potential with soft-wall potential boundaries. In contrast to this, the Si-SiO_2 interface used in Si SETs can produce large and sharp potential discontinuity.

To overcome this problem, we recently proposed and fabricated a novel GaAs SET based on Schottky in-plane-gate (IPG) control of a two-dimensional electron gas (2DEG).[13] In this structure, electric fields are perpendicular to the 2DEG edge and realize stronger confinement than the split gate geometry. The fabricated SET showed Coulomb blockade (CB) oscillation up to 20 K.[13]

The purpose of this paper is to fabricate and characterize single-dot and multiple-dot SETs based on control of a 2DEG with novel Schottky gate

geometries. The previously proposed Schottky IPG and newly introduced Schottky wrap-gate (WPG) geometries were used to realize 1, 2, 3, 18 and 37-dot SETs by electron beam (EB) lithography on AlGaAs/GaAs wafers.

All the devices showed CB-like conductance oscillation with the gate voltage. In single-dot SETs, strong correlation was found between the device dimensions and the temperature limit of the conductance oscillation. The conductance oscillation characteristics of the multiple-dot SETs were complicated. They could not be explained by the classical CB theory. Based on a simplified theoretical analysis using computer simulation, it was shown that energy quantization due to electron confinement and dot-coupling could dominate the charging effect in the fabricated SETs.

2. Sample Structure and Fabrication Process

2.1 *Basic structure and operation principle*

The basic structures and principles for single- and multiple-dot SETs utilizing Schottky in-plane-gate (IPG) and wrap-gate (WPG) geometries are schematically shown in Figs. 1(a)-1(f). Figure 1(a) shows a cross section of the Schottky IPG structure recently proposed by our group.[14] Schottky IPGs form direct contact with the edge of the 2DEG and can control the electric field perpendicular to the edge of the 2DEG plane. Then, they produce strong and efficient confinement of electrons. The quantum wire realized by the Schottky IPGs showed quantized conductance up to 100 K, which is higher than the maximum temperature at which quantized conductance occurs in split-gate

structures.[14-17] The Schottky WPG structure in Fig. 1(b) is also possible and may be more useful in some applications of SETs.

Various types of SETs utilizing the Schottky IPGs and WPGs studied in this paper are shown in Figs. 1(c)-1(f). In these structures, dot sizes and tunneling barriers are voltage-tunable, allowing various conventional operations as well as "turnstile" operations. Figure 1(c) shows a single-dot IPG SET having two finger gates and one main gate. In this structure, tunnel barrier and dot size can be controlled by the finger gates and the main gate, respectively. Figure 1(d) shows a double-dot SET. This device has three finger gates. By changing of the middle finger gate bias, the tunnel barrier between two dots can be controlled. The devices in Figs. 1(e) and 1(f) are 3-dot and multiple-dot WPG SETs, respectively, having multiple-finger gates for tunnel barrier control or dot size control. The multiple-dot SET may be operated, for example, as a "single-electron shift register". Other more complex functional devices seem to be feasible through appropriate design of 2DEG bars, IPGs and WPGs.

2.2 *Device fabrication process*

In this study, the single- and double-dot IPG SETs and 3, 18 and 37 multiple-dot WPG SETs shown in Figs. 1 were fabricated. The device fabrication process is shown in Fig. 2. First, the $Al_{0.3}Ga_{0.7}As$/GaAs double-heterostructure in Fig. 2(a) was grown by standard MBE growth technique at a substrate temperature of 600°C. The thicknesses of the undoped-AlGaAs barrier layer and spacer were 50 nm and 10 nm, respectively. A Si δ- doping layer was inserted between these two layers. The GaAs quantum well thickness was 20 nm and the lower AlGaAs

barrier thickness was 50 nm. On this structure, the SiO_2 passivation layer was formed using a photo-CVD technique. After the formation of the basic structure, 2DEG bar and source and drain pad regions were formed by EB lithography and wet chemical etching, as shown in Fig. 2(b). Then, Au/Ge/Ni ohmic contacts were formed. Finally, Schottky IPG or WPG electrodes at 130~600 nm intervals were defined by EB lithography, and formed either by Pt plating using the *in-situ* electrochemical process for the IPG structures in Fig. 2(c)[18] or by a conventional Cr/Au lift-off process after removal of the SiO_2 layer for the WPG structures in Fig. 2(d). Plan-view SEM images of the fabricated double-dot IPG SET and 18-dot WPG SET are shown in Fig. 3(a) and 3(b), respectively.

3. Experimentally Observed Transport Characteristics of SETs

3.1 *Conductance oscillation characteristics of single-dot SETs*

We fabricated and characterized the transport of the single-dot SETs in Fig. 1(c) using different device dimensions, devices A~D. Examples of the observed conductance oscillations of devices C and D are shown in Figs. 4(a) and 4(b), respectively. All of the single-dot SETs showed clear conductance oscillation characteristics.____ It is also noted in Fig. 4(b) that the current becomes negative at a certain gate voltage. This point will be discussed at the end of §3.2, because such a phenomenon was also observed in multiple-dot SETs. Conductance oscillation in device D with finger gate spacing d_F of 200 nm was visible up to 30 K, which is much higher than the maximum temperature T_{max} of conductance oscillation for the split-gate SETs. The observed Coulomb gap ΔV_{Σ} of device D

was 10 mV, also corresponding to the observed T_{max} of 30 K.

The observed conductance oscillation characteristics and device dimensions are summarized in Table I. A strong correlation between T_{max} and the device dimensions was found. T_{max} increases markedly with a decrease in the device dimensions. Since the effective channel width can be changed by changing of the main gate bias V_{GM}, d_F directly reflects the dot size and charging energy U, as seen by the simple relationship of $k_B T_{max} \sim U = e^2/C_\Sigma \sim 1/d_F$. From this relationship, further reduction of finger gate spacing 50 nm should allow 77-300 K operation of the novel SETs.

3.2 *Conductance oscillation characteristics of multiple-dot SETs*

Figures 5(a) and 5(b) show the conductance oscillation on the double-dot SET in Fig. 2(d) for different finger gate bias conditions. In this device, a 2DEG bar width W of 780 nm, finger gate spacing d_F of 200 nm and metal finger gate width L_{GF} of 200 nm were realized. It was seen that the behavior of the conductance oscillation was changed by changing of the gate bias condition. In the case of the high negative finger gate bias condition as shown in Fig. 5(a), doublet peaks due to interdot coupling were observed, which corresponded to the behavior expected from the classical capacitive charging model.[2] On the other hand, in the low negative finger gate bias condition as shown in Fig. 5(b), 4-pair peaks were observed near the drain current pinch-off, which could not be explained by the classical model. This indicates the effect of quantization energy due to electron confinement. The oscillation behavior became stochastic with an increase in the main gate bias V_{GM}. By sweeping of the middle finger gate bias V_{GF2}, the

position of each 4-pair peak changed, but not monotonously.

Figure 6(a) shows the conductance oscillation characteristics of the 3-dot WPG SET. The device dimensions were W=1,200 nm, d_F=130 nm and L_{GF}=70 nm. This device showed unique characteristics. Fine conductance oscillation peaks with a period of 2.0~2.5 mV were observed. Six of these peaks seemed to be defined as a group with a period of about 10 mV. This behavior could not be explained by the classical capacitive charging model which predicted triplet peak separation by a 3-dot device.[2] The peaks in each group showed nearly the same amplitude of conductance. The amplitude decreased exponentially with a decrease in the gate voltage, such as $0.2e^2/h \varnothing 0.1e^2/h \varnothing 0.04e^2/h \varnothing 0.02e^2/h$, where e^2/h is quantized conductance unit. Figure 6(b) shows the I_{DS}-V_{DS} characteristics of the 3-dot SET. In these characteristics, the voltage gaps which seemed to be a Coulomb gap could be clearly seen at certain gate biases. These gaps changed with an increase in the gate voltage. The maximum value of the observed gap was about 5 mV. A negative resistance characteristic was also observed when $|V_{DS}|$>5 mV. This characteristic seems to be due to resonant tunneling through quantized levels due to electron confinement in the dots.[19]

Conductance oscillation characteristics of 18-dot and 37-dot WPG SETs are shown in Figs. 7(a) and 7(b), respectively. The device dimensions were W=770 nm, d_F=170 nm and L_{GF}=30 nm for the 18-dot SET and W=1,300 nm, d_F=160 nm and L_{GF}= 40 nm for the 37-dot SET, respectively. These multiple-dot SETs showed clear and regular conductance oscillations compared to the 3-dot SET, and behaved essentially like a single-dot SET. The conductance oscillation of the 18-dot SET in Fig. 7(a) was observed up to 15 K even when V_{DS}=1 mV. The conductance oscillation of the 37-dot SET in Fig. 7(b) could be observed at 5 K, even if the

channel width was as wide as 1,300 nm.

Finally, as seen in Figs. 5(a), 5(b) and 7(b), the multiple-dot SETs often showed negative currents despite a positive drain-source voltage, as in the case of the single-dot SET shown in Fig. 4(b). Similar conductance characteristics were observed previously by other investigators for AlGaAs/GaAs longitudinal RTD SETs[19)] and Si MOS SETs[20)], although the presence of such a phenomenon and its mechanism were not discussed.

In the present study, many of the fabricated SETs showed such surprising and mysterious current characteristics. The general features can be summarized as follows. (1) The characteristics are reproducible. (2) At the gate voltage giving rise to a negative current, the corresponding I_{DS}-V_{DS} curve shows a small horizontal shift in the positive voltage direction, indicating the presence of an effective "off-set" voltage to V_{DS}. (3) By changing of the polarity of V_{DS}, an I_{DS}-V_{G} characteristics without negative currents is obtained. This agrees with the above point (2). (4) At large negative gate voltages, the SET is completely pinched off and no negative current peaks appear. (5) When the total current becomes large at larger V_{DS} values and higher temperatures, negative currents disappear.

The mechanism for this phenomenon is not clear at present. The possibility of malfunction of the measurement equipment (HP 4156A semiconductor parameter analyzer) was ruled out. One possible mechanism is the charging of surface states or bulk trap states in the depletion layer which are charged at a particular gate bias. Since the devices have high resistances (10~100 MΩ), the charging effect remains unscreened at low current levels and effectively produces an offset voltage to the drain bias. Since this phenomenon seems to be a general phenomenon in semiconductor SETs, further investigation is obviously necessary

to determine its mechanism and means of its removal.

4. Simplified Theoretical Analysis and Interpretation of Experiment Results

4.1 *Simplified theoretical analysis of single-dot SET*

We performed quantitative analysis of the Coulomb blockade characteristics of a single-dot SET by potential simulation and a simple theory. Potential distributions in the Schottky IPG structures were calculated in the classical regime by solving a three-dimensional (3D) Poisson's equation with the successive over-relaxation (SOR) method. The inset of Fig. 8(a) shows a plan view of the calculated potential profile of the single-dot IPG SET, device C in Table I. Formation of a quasi-elliptic dot is clearly seen. The calculated dot size and charging energy as a function of V_{GM} are shown in Fig. 8(a). The dot size was calculated based on the assumption that the area of the dot equaled the area of a circle of radius R. The dot capacitance C_Σ was estimated using $C_\Sigma=8\varepsilon R$, where ε is the permittivity.[12] It was found that the dot size reaches 20 nm and then the charging energy reaches 10 meV by control of V_{GM}. However, this energy is about 4 meV larger than the experimental result. A possible reason for this is that the tunnel barrier becomes large when V_{GM} greatly decreases and electron tunneling becomes impossible before the dot size is reduced to such a small size.

Peak intervals of the conductance oscillation for the single-dot SET were also simulated using the 3D potential calculation. The peak interval $\Delta V_G=V_{G(n+1)\text{-th}}-V_{G(n)\text{-th}}$ was calculated semi-classically using

$$e\,\Delta n = \int_{-\infty}^{V_{G(n)\text{-th}}} C_G(V_G)\,\mathrm{d}V_G \quad , \qquad (1)$$

where n is an integer, e is the element charge of a electron and C_G is the differential gate capacitance. C_G is given by

$$C_G(V) = \frac{\partial Q}{\partial V_G} = e\frac{\partial n_e}{\partial V_G} \quad , \qquad (2)$$

where n_e is the number of electrons in the dot. n_e is counted classically by applying the 3D density of states. The gate voltage that satisfies eq. (1) gives the n-th conductance peak. The relationship between ΔV_G and peak number, j, from the experiment and theory for a single-dot SET (device C) is shown in Fig. 8(b). Reasonably good semi-quantitative agreement was obtained between the theoretical and experimental results. However, some irregularity was seen in the experimental data. This indicates that the effect of quantization energy due to electron confinement is revealed even when d_F=400 nm. Such irregularity seems to occur when the quantized energy state that the electron passes changes. Additional investigation, including self-consistent analysis of the quantum mechanical effect and electrical potential, is needed for full understanding of the experimental results.

4.2 *Interpretation of conductance oscillation of multiple-dot SETs*

4.2.1 *Double-dot IPG SET*

We observed two different behaviors of conductance oscillation in the double-dot IPG SET. This difference indicates that the transport mechanism changes with the change in the finger gate bias condition, which seems to

correspond to the two models in Fig. 9 for the conductance oscillation of double-dot SETs. Figure 9(a) schematically shows the classical capacitive charging model for peak splitting due to interdot coupling in a double-dot SET.[2)] This model is applicable when the charging energy U is larger than the quantized energy ΔE due to electron confinement. Each zero interdot coupling eigenstate with a definite particle number N on each dot gives rise to a parabola. The center parabola which corresponds to the condition that an odd number of electrons are in the system as indicated by (N,N+1) or (N+1,N) in Fig. 9(a) is shifted down by interdot coupling. Then the degenerated states are split and the conductance peak splits into a doublet peak. This model can explain the doublet peaks in Fig. 5(a). On the other hand, when the quantized energy is larger than the charging energy, the transport mechanism changes and the conductance oscillation is dominated by quantized energy due to electron confinement and the conductance peak position is corrected by the charging energy, as shown in the model in Fig. 9(b).[3-5)] In the two-dot system, quantized eigenstates due to electron confinement are degenerated in each quantized level. The number of degenerated states equals the product of the number of dots and spin degeneracy, so this system can be treated as a virtual one-dot system having 4-fold degenerated states at each quantized level, as shown in Fig. 9(b). The degenerated eigenstates in the dot are separated by interdot coupling energy T and charging energy U. Therefore, in the double-dot device, the conductance peak from each quantized level splits into 4-pair peaks, which explains the result in Fig. 5(b).

From the gate bias condition, the dot size in Fig. 5(a) was expected to be smaller than that in Fig. 5(b).[13)] Then, it seemed that the quantized effect was more dominant in Fig. 5(a). However, as shown in Fig. 8(a), when the dot becomes

sufficiently small, it is possible that the charging energy becomes larger than the quantized energy. Thus, the oscillation characteristics in Fig. 5(a) are dominated by the charging effect and the behavior is close to that expected from the classical model in Fig. 9(a). The shift of each peak in the pair observed in Fig. 5(b) was not monotonous with the change of V_{GF2}, which corresponds to a decrease in the tunneling probability. On the other hand, it was reported that the interdot coupling energy T also depended on the dot size, and indicated that T increased with a decrease in dot size.[3)] In the present double-dot SET structure, the dot size was also changed by a decrease in V_{GF2}. Therefore, the observed behavior of peak positions seemed to be possible because the position of each peak was determined by the balance between U and T.[3-5)]

4.2.2 *3, 18 and 37-dot WPG SETs*

In the present 3, 18 and 37-dot WPG SETs with the structure shown in Figs. 1(e) and 1(f), d_F were as narrow as 130~170 nm. And since these devices did not have main gates to control the effective wire width, the dot size could not be smaller than those for the present single- and double-dot IPG SETs. Thus, in the case of the present 3, 18 and 37-dot WPG SETs, ΔE is expected to be larger than U. Figure 10(a) shows the estimated U and ΔE as a function of the gate voltage from the potential simulation for the 3-dot WPG SET. The ΔE is 5~6 meV, which is about 5 times larger than U.

The grouping of conductance oscillation peaks in the 3-dot SET is considered to be brought about by the situation that the quantized energy is greater than the charging energy. In this case, based on the model in Fig. 9(b), the 3-dot system can be treated as a one-dot system having 6-fold degenerated states. The

degenerated states are separated by charging energy and interdot coupling, which results in 6 peaks in one quantized level, as shown in Fig. 10(b). The nearly identical amplitudes of the peaks in each group indicates that the transition probability depends strongly on the quantized energy level as schematically shown in Fig. 10(b). The difference in the dot to lead transition probability for each quantized level seems to cause this situation.

For detailed analysis of the oscillation behavior of multiple-dot WPG SETs when $\Delta E>U$, we estimated the peak separation due to interdot coupling and charging effects by the Hubbard model.[3-5] The exact solution of the Hamiltonian shows that conductance peaks from one quantized energy level have two groups separated roughly by U which correspond to the Hubbard band, and each group contains a number of peaks separated by interdot coupling equal to the number of dots, when $U>T$.[4] Therefore, we have only to solve the next equation to estimate peak separation by the interdot coupling effect, assuming $U>T$,

$$\det|H-E|=\begin{vmatrix} E_n-E & T & 0 & \cdots \\ T & E_n-E & T & \cdots \\ 0 & T & E_n-E & \cdots \\ \vdots & \vdots & \vdots & \ddots \end{vmatrix}=0 , \qquad (3)$$

where E is the eigenenergy and E_n is n-th quantized energy. The number of columns and rows in the matrix given by eq. (3) corresponds to the number of dots in an array. For example, all of the eigenstates including the charging energy U become $E=E_n \pm T$, $E_n+U\pm T$ for the two-dot system and $E=E_n$, $E_n \pm T\sqrt{2}$, E_n+U, $E_n+U\pm T\sqrt{2}$ for the three-dot system.

From the observed Coulomb gap and the potential simulation of the 3-dot SET, the charging energy is estimated to be about 1~2 meV. Interdot coupling

energy can be estimated using $T \sim 4h^2/m^*d^2$, where m^* is the effective electron mass and d is the dot size.[3] T is estimated to be about 0.3~0.4 meV for the 3-dot SET. These estimated values can explain the nearly equal spacing of the fine peaks in the conductance oscillation of the 3-dot SET. The calculated peak separation by the interdot coupling and charging effect from one quantized energy level is shown in Fig. 11 for various numbers of dots, assuming U:T=1:0.4. As shown in this figure, the larger the number of dots becomes, the narrower the separation of peaks becomes with the same interdot coupling energy. The peak separation can be observed when the peak interval is larger than thermal broadening. When T is 0.3~0.4 meV, it is found that the peak separation can be observed within a few Kelvin for the 3-dot SET, but not for the 18- and 37-dot SETs. Therefore, when the number of dots in a multiple-dot SET increases, the fine peaks due to interdot coupling are smeared out and conductance oscillation may be simplified compared to that of the 3-dot SET. However, if we can control the interdot coupling and charging energy of each dot independently, it will be possible to observe a more interesting peak separation behavior in the conductance oscillation of multiple-dot SETs.

5. Conclusion

Single-dot and multiple (2, 3, 18 and 37)-dot SETs based on the control of a two-dimensional electron gas (2DEG) with Schottky in-plane-gate (IPG) and wrap-gate (WPG) geometries were fabricated on AlGaAs/GaAs heterostructures by EB lithography, and their transport properties were characterized. The main conclusions are listed below.

(1) All the fabricated SETs showed Coulomb blockade-like conductance oscillation with the gate voltage.

(2) Single-dot SETs realized by Schottky IPG could be operated of high temperatures up to 30 K. Fabricated single-dot SETs show a strong correlation between device dimensions and temperature limit of conductance oscillation, which indicates that higher temperature operation can be achieved by optimization of the device dimensions.

(3) Simplified theoretical analysis based on computer simulation was performed for a single-dot SET and semi-quantitative agreement was obtained between the theoretical and experimental results. Some irregularity in the experimental results indicates an interplay between the energy quantization due to electron confinement and the charging effect.

(4) The double-dot SET showed peak separation due to interdot coupling in the conductance oscillation. Doublet or 4-pair peaks were observed upon changing of the gate bias condition. This shows that the relationship between the charging energy and quantized energy was changed by changing of the gate bias condition.

(5) The 3-dot SET with a reduced inter-gate dimension of 130 nm exhibited a 6-pair peak in the conductance oscillation indicating that the quantized energy is dominant over the charging energy. On the other hand, 18- and 37-dot SETs behaved essentially like single-dot SETs above 1.9K due to the smearing out of fine energy separations by thermal broadening.

References

1) H. van Houten, C. W. J. Beenakker and A. A. M. Staring: *NATO Advanced Study Institute, Series B: Physics*, eds. H. Garbert and M. H. Devoret (Plenum, New York, 1992) Vol.294.

2) F. R. Waugh, M. J. Berry, D. J. Mar, R. M. Westervelt, K. L. Campman and A. C. Gossard: Phys. Rev. Lett. **75** (1995) 705.

3) C. A. Stafford and S. D. Sarna: Phys. Rev. Lett. **72** (1994) 3590.

4) G. Chen, G. Klimeck, S. Datta, G. Chen and W. A. Doddard III: Phys. Rev. B **50** (1994) 8035.

5) G. Klimeck, G. Chen and S. Datta: Phys. Rev. B **50** (1994) 2316.

6) I. M. Ruzin, V. Chandrasekhar, E. I. Levin and L. I. Glazman: Phys. Rev. B **45** (1992) 13469.

7) K. K. Likharev, N. S. Bakhvalov, G. S. Kazacha and S. I. Serdyukova: IEEE Trans. Magn. **25** (1989) 1436.

8) L. J. Geerligs, V. F. Anderegg, P. A. M. Holweg, J. E.Mooji, H. Pothier, D. Esteve, C. Urbina and M. H. Devoret: Phys. Rev. Lett. **64** (1990) 2691.

9) K. Yano, T. Ishii, T. Hashimoto, T. Kobayashi, F. Murai and K. Seki: IEEE Trans. Electron Devices **41** (1994) 1628.

10) Y. Takasahi, M. Nagase, H. Namatsu, K. Kurihara, K. Iwadate, Y. Nakajima, S. Horiguchi, K. Murase and M. Tabe: Electron. Lett. **31** (1995) 136.

11) U. Merirav, M. A. Kastner, and S. J. Wind: Phys. Rev. Lett. **65** (1990) 771.

12) L. P. Kouwenhoven, N. C. van der Vaart, A. T. Johnson, W. Kool, C. J. P. M. Harmans, J. G. Williamson, A. A. M. Staring and C. T. Foxon: Z. Phys. B **85** (1991) 367.

13) K. Jinushi, H. Okada, T. Hashizume and H. Hasegawa: Jpn. J. Appl. Phys. **35**

(1996) 397.

14) H. Okada, K. Jinushi, N.-J. Wu, T. Hashizume and H. Hasegawa: Jpn. J. Appl. Phys. **34** (1995) 1315.

15) H. Hasegawa, T. Hashizume, H. Okada and K. Jinushi: J. Vac. Sci. & Technol. B **13** (1995) 1744.

16) H. Okada, T. Hashizume and H. Hasegawa: Jpn. J. Appl. Phys. **34** (1995) 6971.

17) T. Hashizume, H. Okada and H. Hasegawa: *Tech. Dig. 3rd Int. Symp. on New Phenomena in Mesoscopic Structure*, Maui, December, 1995, Q16.

18) T. Hashizume, G. Schweeger, N.-J. Wu and H. Hasegawa: J. Vac. Sci. & Technol. B **12** (1994) 2660.

19) S. Tarucha, D. G. Austing and T. Honda: Supperlattices & Microstructures **18** (1995) 121.

20) H. Matsuoka and S. Kimura: Jpn. J. Appl. Phys. **34** (1995) 1326.

Figure captions

Fig.1. Principles and basic structures of SETs utilizing Schottky IPGs and WPGs.

Fig.2. Device fabrication process.

Fig.3. SEM images of (a) a double-dot IPG SET and (b) an 18-dot WPG SET.

Fig.4. Conductance oscillations of single-dot IPG SETs in (a) device C and (b) device D.

Fig.5. Conductance oscillations of the double-dot IPG SET device for different gate bias conditions.

Fig.6. (a) Conductance oscillations and (b) I_{DS}-V_{DS} characteristics of the 3-dot WPG SET.

Fig.7. Conductance oscillations of (a) 18-dot and (b) 37-dot WPG SETs.

Fig.8. (a) Simulated dot size and charging energy and (b) comparison of conductance peak separations between theory and experiment for a single-dot IPG SET (device C).

Fig.9. Transport models for a double-dot SET in the cases of (a) $U > \Delta E$ and (b) $U < \Delta E$.

Fig.10. (a) Calculated ΔE and U and (b) the conductance oscillation model for the 3-dot WPG SET.

Fig.11. Calculated peak separation by interdot coupling and the charging effect for various numbers of dots.

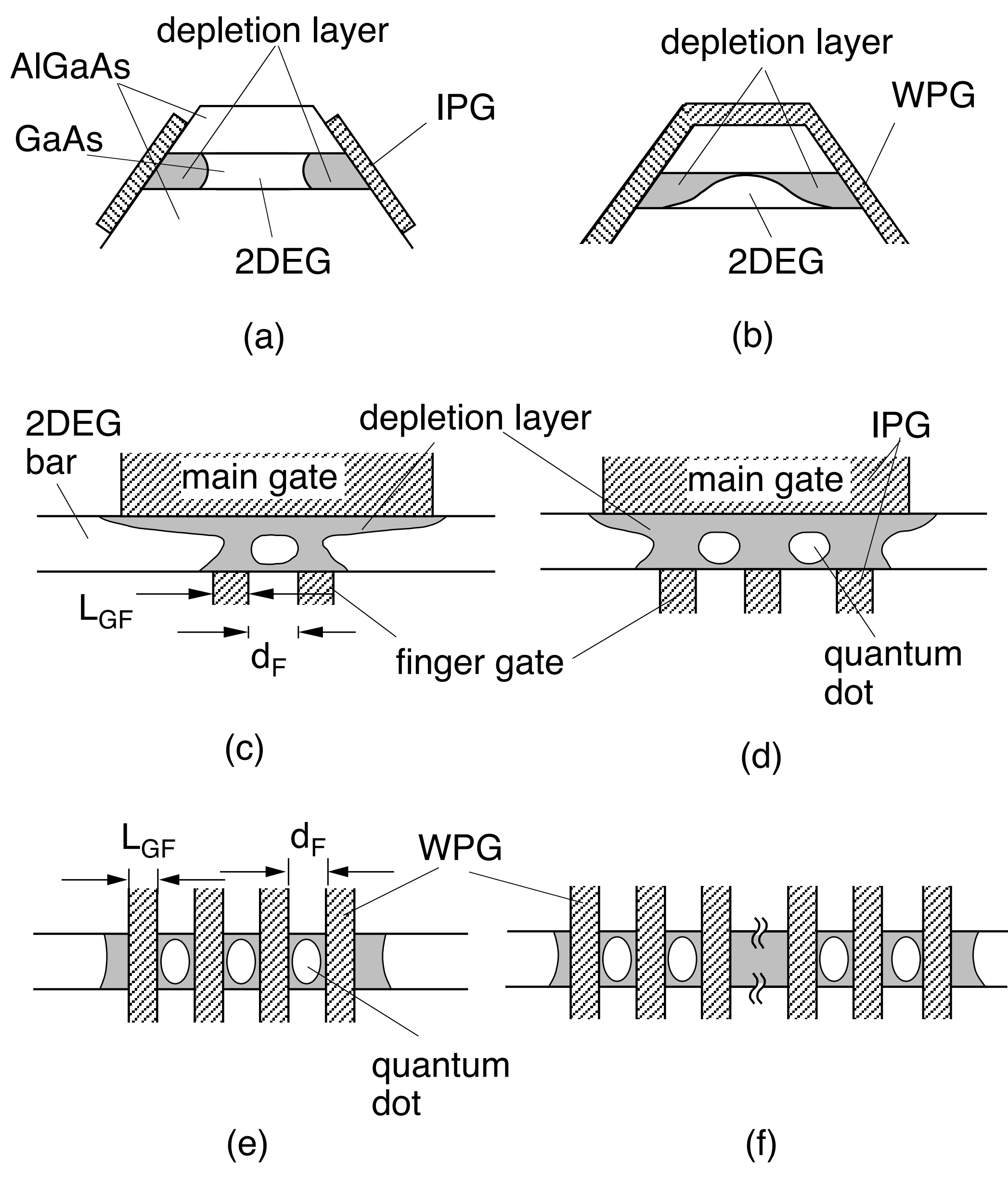

Figure 1

S. Kasai et al.

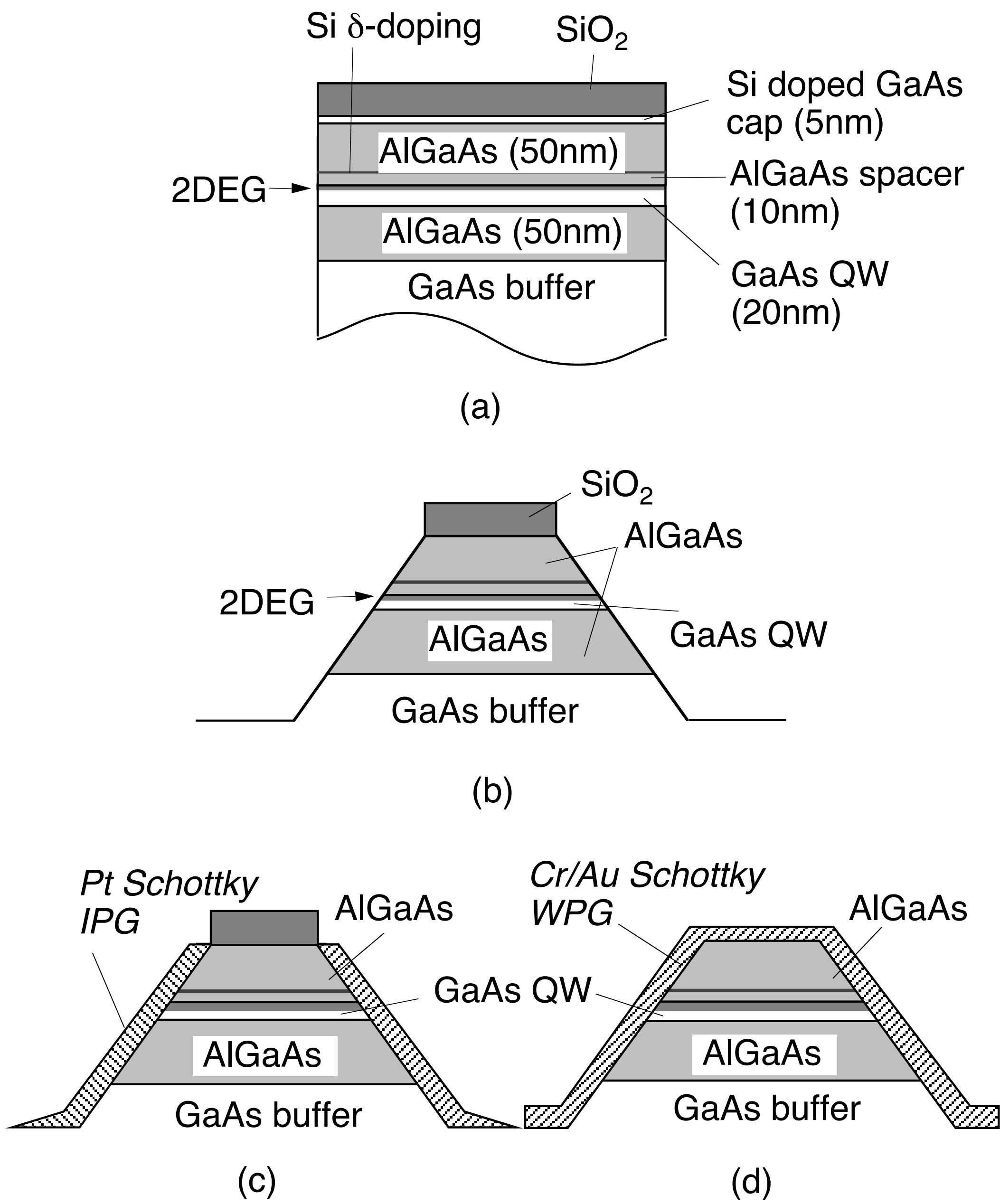

Figure 2

S.Kasai et al.

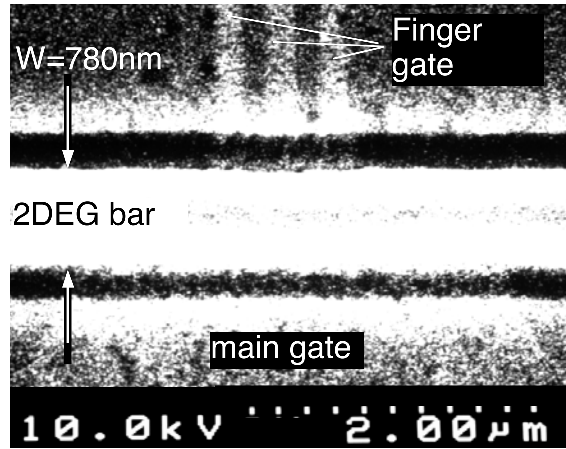

(a)

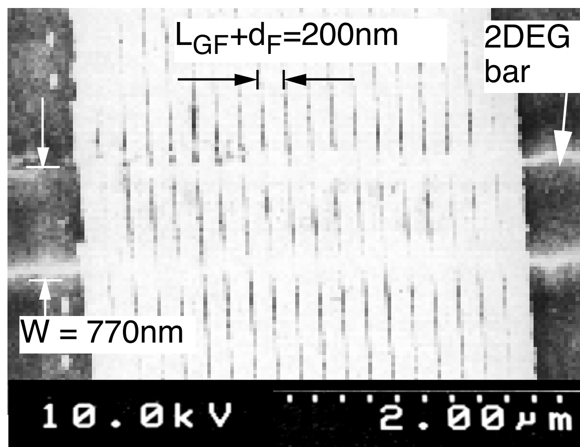

(b)

Figure 3

S.Kasai et al.

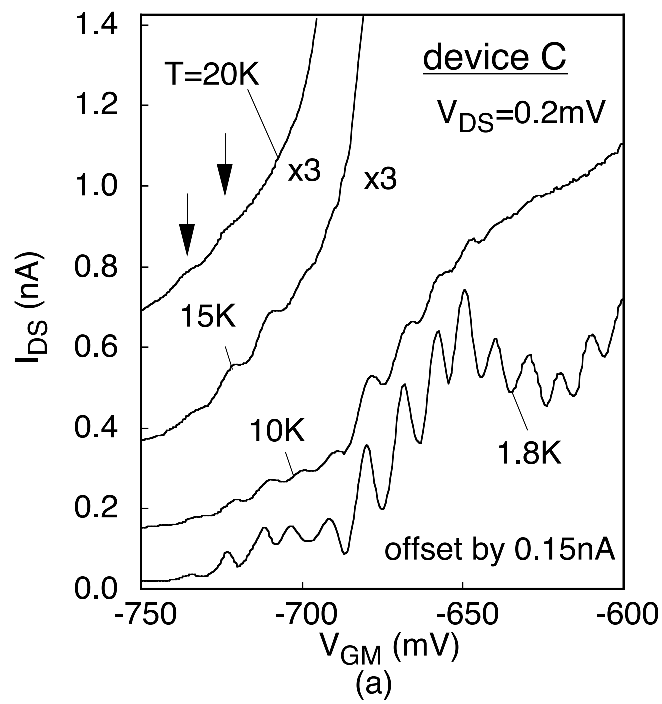

(a)

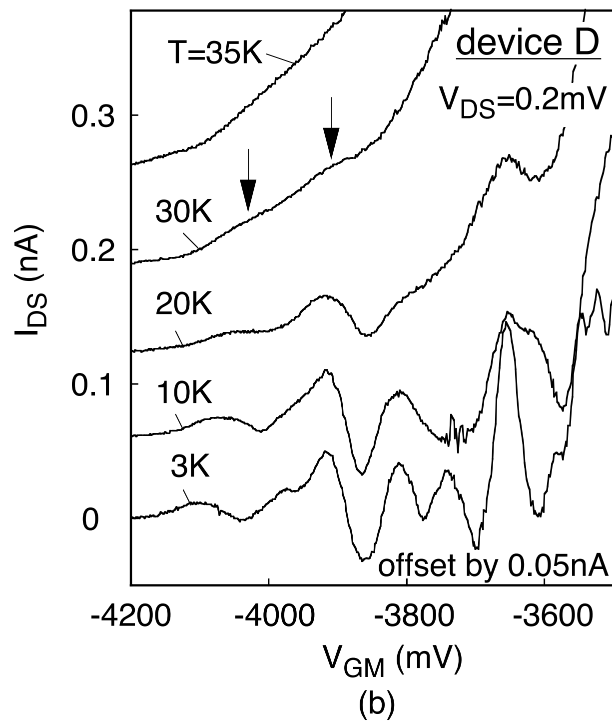

(b)

Figure 4

S.Kasai et al.

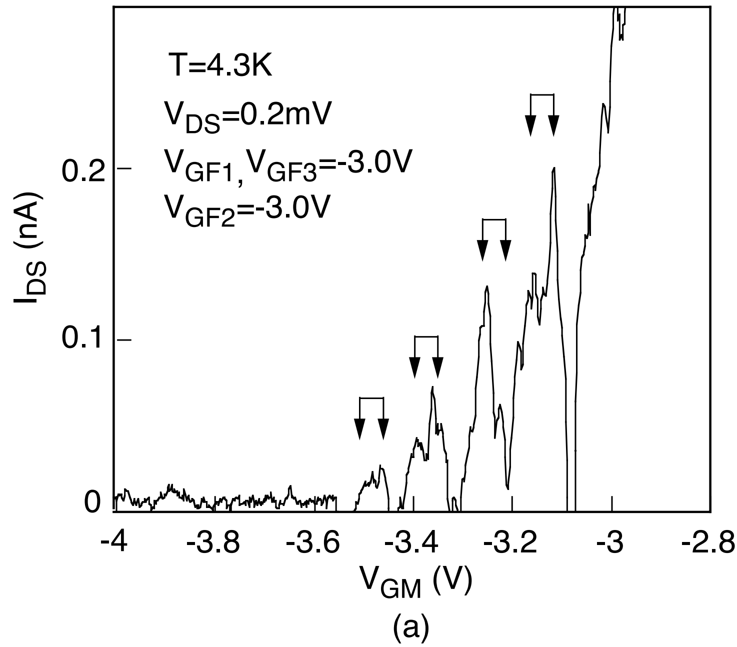

(a)

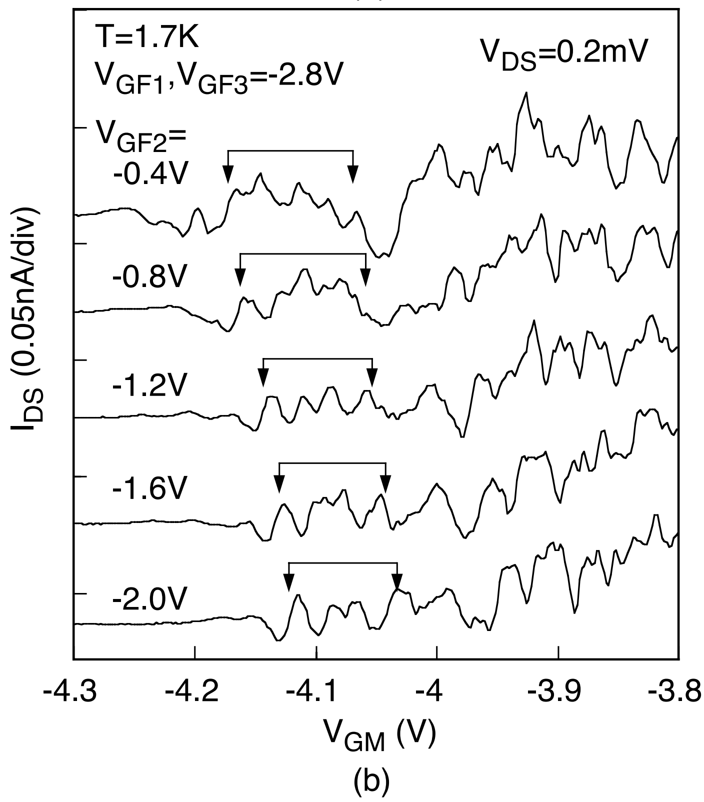

(b)

Figure 5

S.Kasai et al.

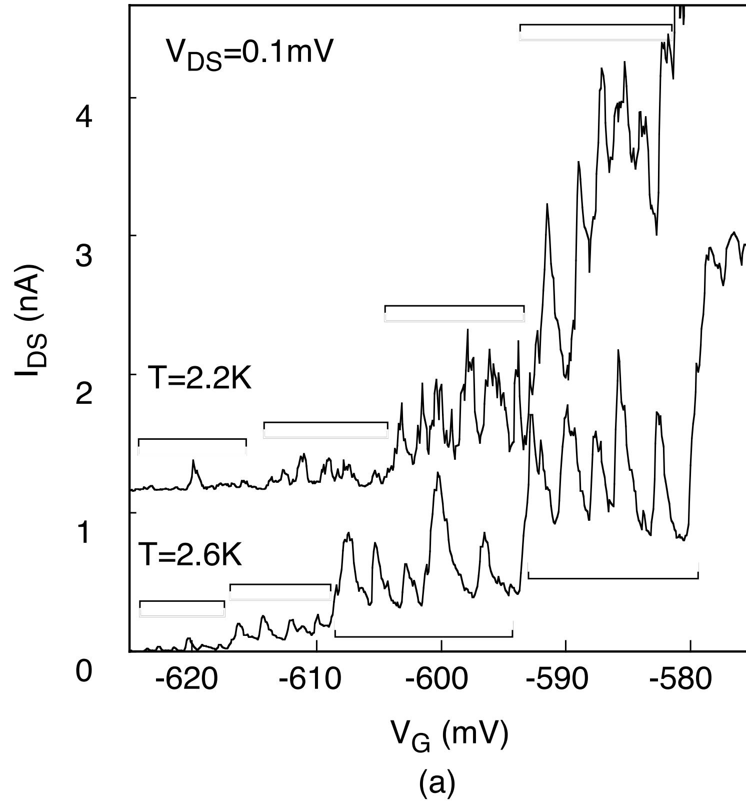

(a)

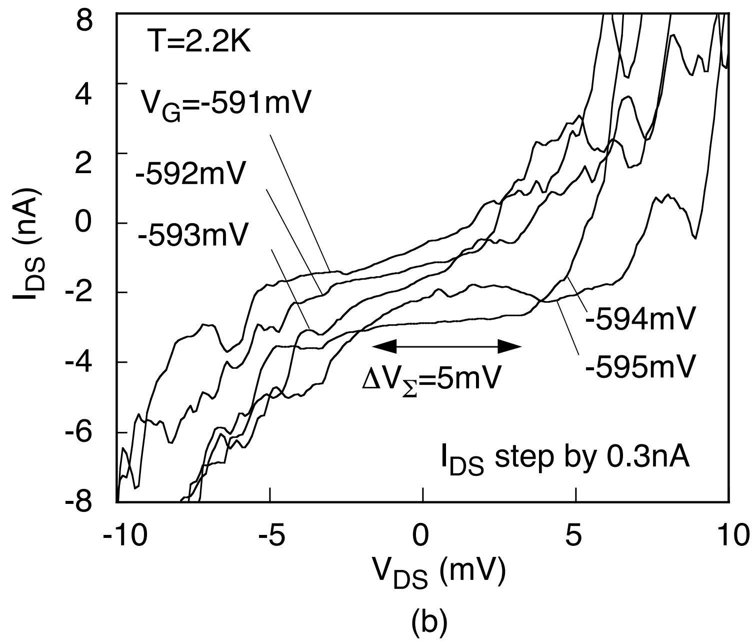

(b)

Figure 6

S.Kasai et al.

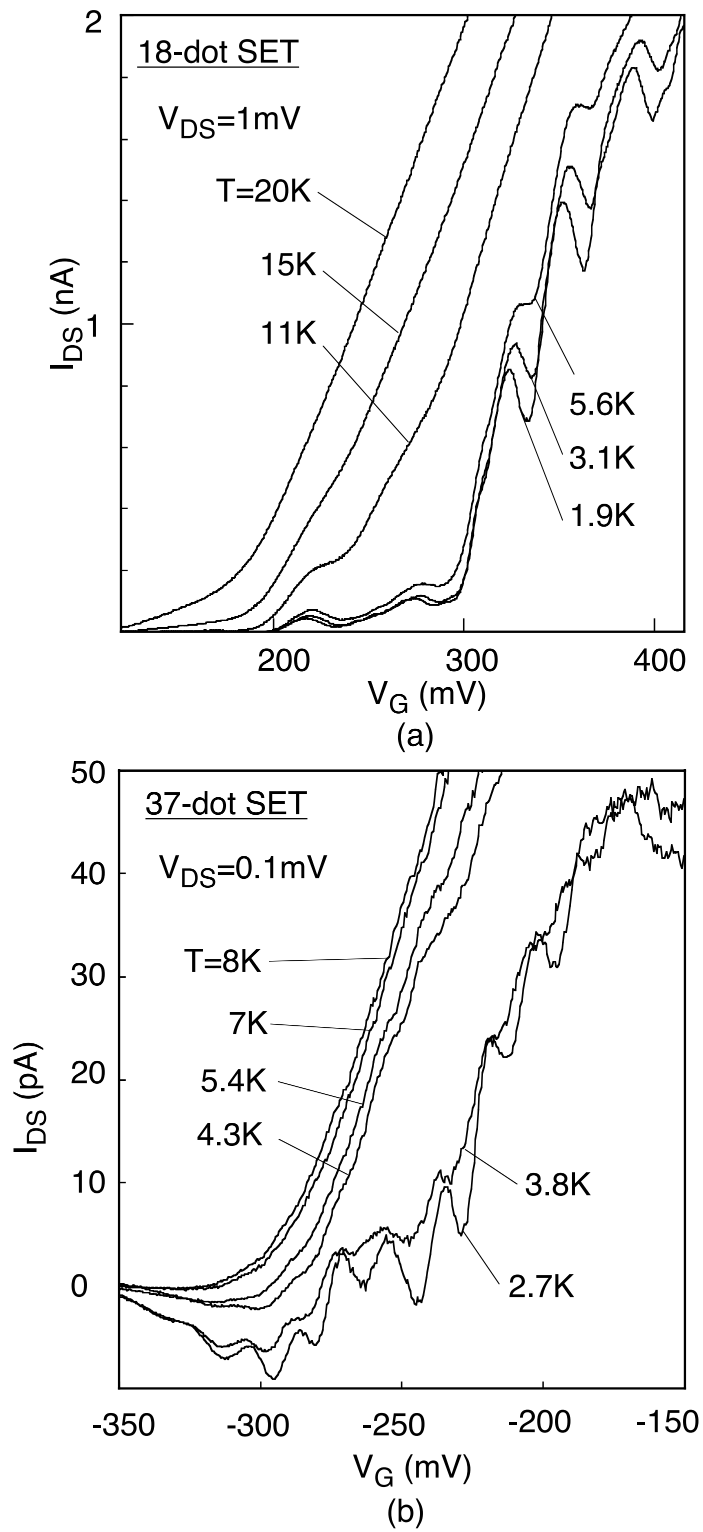

Figure 7

S. Kasai et al.

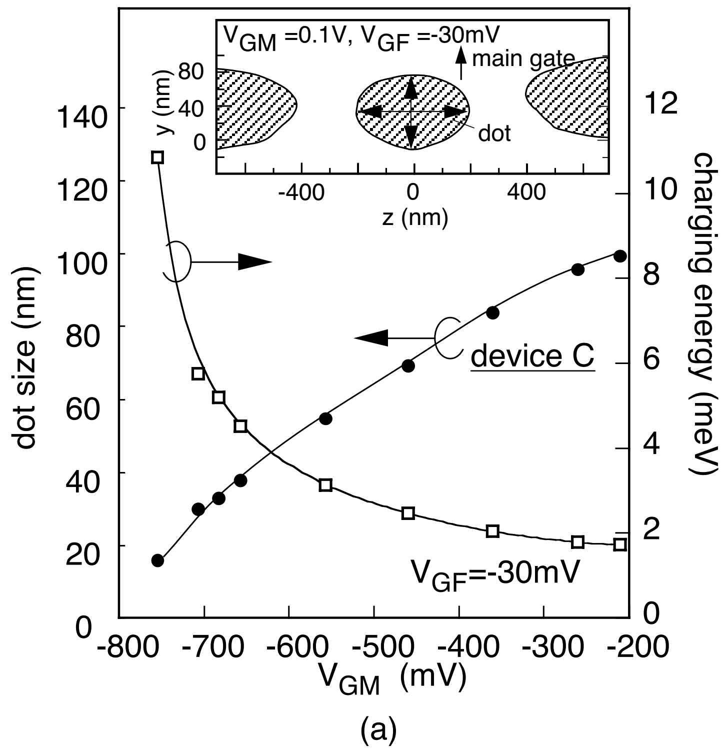

(a)

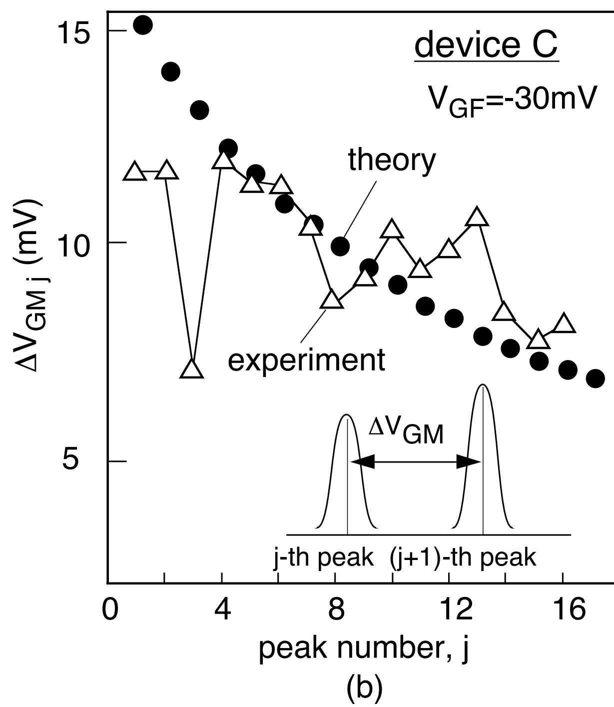

(b)

Figure 8

S.Kasai et al.

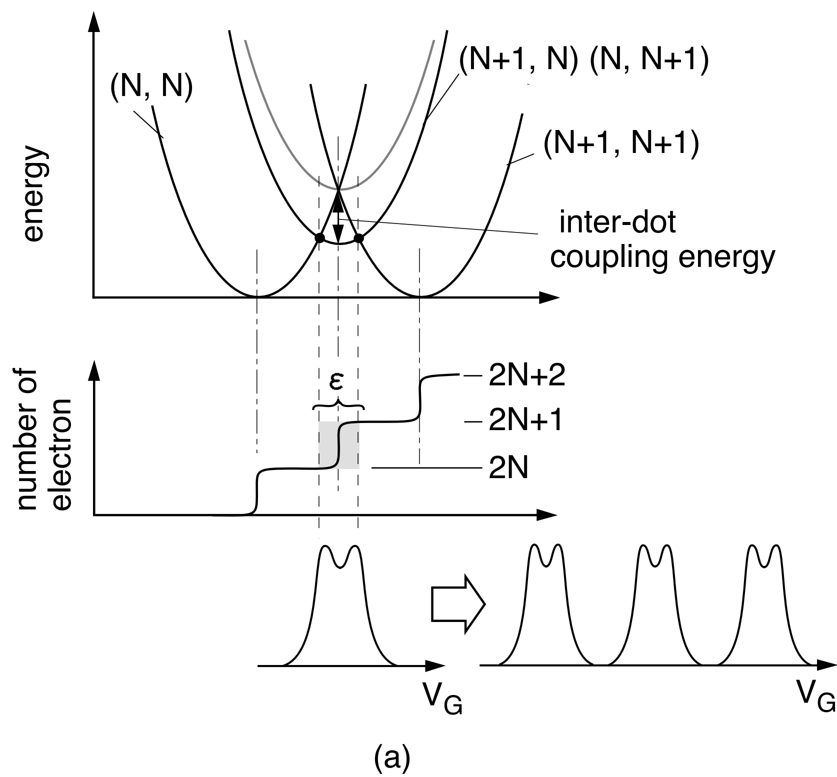

(a)

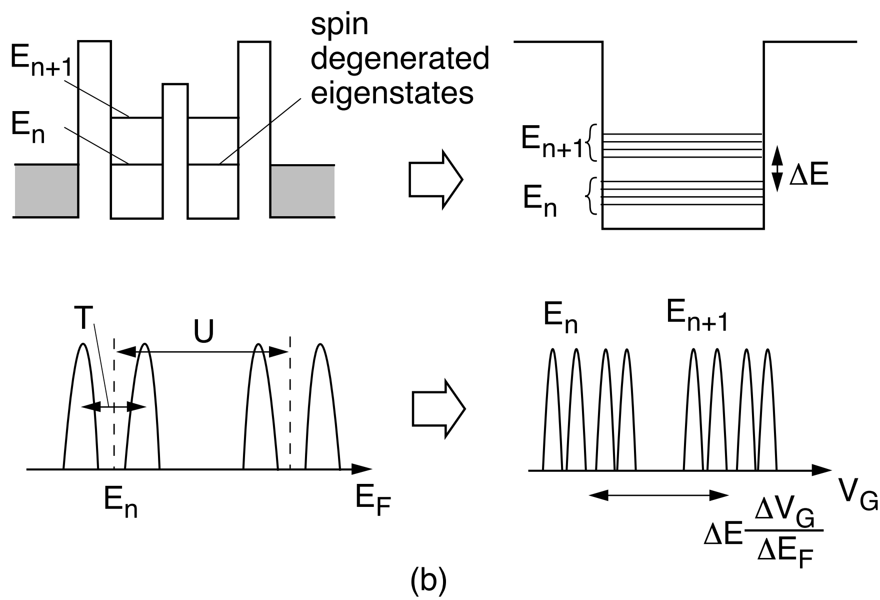

(b)

Figure 9

S.Kasai et al.

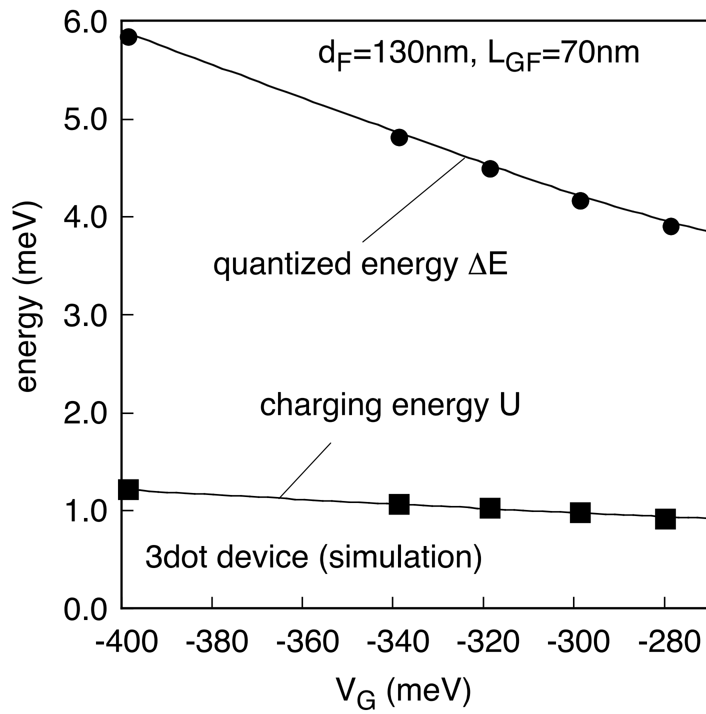

(a)

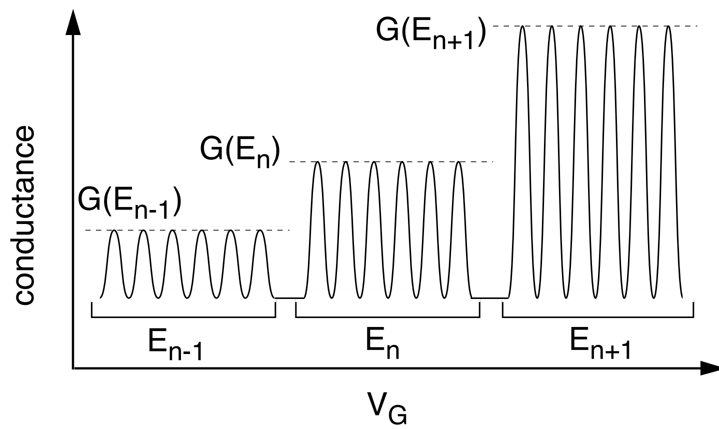

(b)

Figure 10

S.Kasai et al.

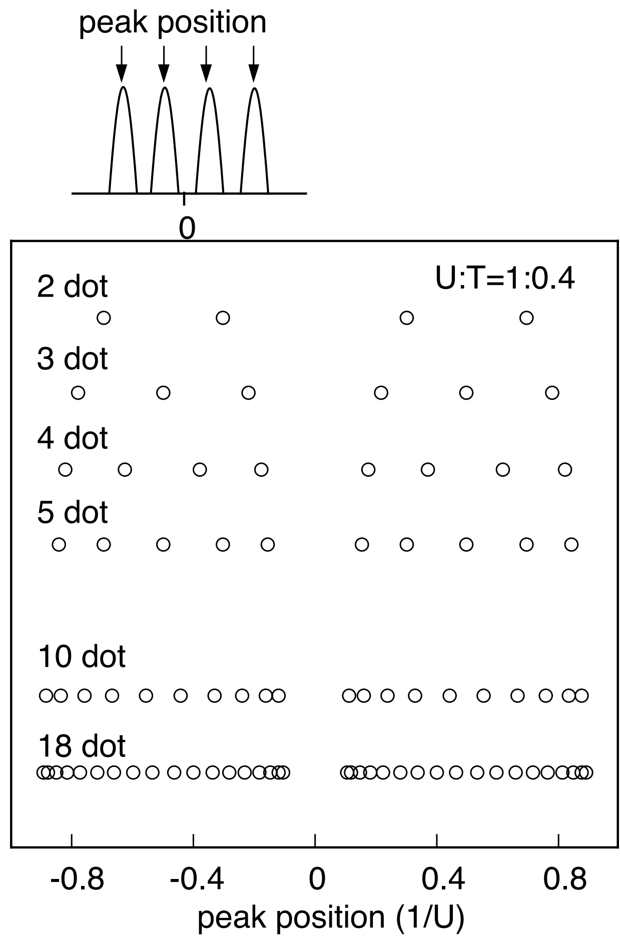

Figure 11

S.Kasai et al.

Table I
Device dimensions and conductance oscillation characteristics of single-dot SET devices.

device	d_F (nm)	L_{GF} (nm)	W (nm)	ΔV_G (mV)	ΔV_Σ (mV)	T_{max} (K)
A	600	400	600	5~10	–	3.4
B	600	200	800	10~20	–	10
C	400	200	550	10~15	6	20
D	200	200	600	70~100	10	30

ΔV_G (mV): conductance oscillation period
ΔV_Σ (mV): observed Coulomb gap
T_{max} : maximum temperature of conductance oscillation